Letter

Intrinsic and doping-enhanced superconductivity in monolayer 1*H*-TaS_2: Critical role of charge ordering and spin-orbit coupling

Chao-Sheng Lian,[1,*] Christoph Heil,[2] Xiaoyu Liu,[3] Chen Si,[4] Feliciano Giustino,[5,6] and Wenhui Duan[3,7]

[1]*School of Physics and Microelectronics, Zhengzhou University, Zhengzhou 450001, China*
[2]*Institute of Theoretical and Computational Physics, Graz University of Technology, NAWI Graz, 8010 Graz, Austria*
[3]*Institute for Advanced Study, Tsinghua University, Beijing 100084, China*
[4]*School of Materials Science and Engineering, Beihang University, Beijing 100191, China*
[5]*Oden Institute for Computational Engineering and Sciences, The University of Texas at Austin, Austin, Texas 78712, USA*
[6]*Department of Physics, The University of Texas at Austin, Austin, Texas 78712, USA*
[7]*Department of Physics and State Key Laboratory of Low-Dimensional Quantum Physics, Tsinghua University, Beijing 100084, China*

(Received 16 June 2021; accepted 17 May 2022; published 24 May 2022)

The interplay of superconductivity with charge density wave (CDW) in metallic transition-metal dichalcogenides has been widely debated, and viable strategies manipulating these quantum states in the two-dimensional (2D) limit remain unclear. Using the *ab initio* anisotropic Migdal-Eliashberg theory, we successfully explain the superconductivity observed in monolayer 1*H*-TaS_2 by simultaneously determining its precise CDW structure and treating the marked modification of electron-phonon interaction and critical temperature T_c by spin-orbit coupling effects. With this paradigm, we further show that electron doping weakens the CDW order leading to increased T_c up to 11 K, along with a single-gap to two-gap superconductivity transition due to the suppression of the CDW gap. By contrast, a low hole doping barely affects the CDW but still yields a significantly enhanced superconducting order, implying their good coexistence. Combined with the synergistic behavior of CDW and superconductivity, which cooperate upon TaS_2 thickness reduction causing an unusual rise of T_c, our results unravel diversified interactions between the two collective orders in ultrathin TaS_2, being competition, coexistence or cooperation depending on external stimuli, which provide key clues for controlling correlated states in devices based on 2D CDW superconductors.

DOI: 10.1103/PhysRevB.105.L180505

Quantum states as superconductivity and charge density wave (CDW) were long studied in transition-metal dichalcogenides (TMDs) [1,2], and interest in their mutual relation has been revitalized since the detection of a CDW in the pseudogap region of high-T_c cuprates [3,4]. One of the most challenging TMDs is TaS_2, which shows multiple CDWs in 1*T* phase or coexisting CDW and superconducting orders in 2*H* phase. While for 1*T*-TaS_2 superconductivity occurs in a textured CDW state complicating interplay of the two orders [5–7], for 2*H*-TaS_2 it gets enhanced once CDW is suppressed by intercalation or weak disorder [8,9], implying an exclusive interaction. Pressurization of 2*H*-TaS_2 could induce further exotic behavior. Transport experiments revealed its CDW lock-in transition from incommensurate to commensurate and a dramatic rise of superconducting T_c with CDW existing up to the highest applied pressure [10]. Later on, Raman and magnetic experiments observed a Higgs mode coupling to its CDW amplitudons [11] and a superconducting dome with a maximum T_c of 9 K [12], but found the CDW to collapse at relatively low pressure. As such, the interplay of collective states in these layered CDW superconductors has become a contemporary research subject in both theory and experiment [13–15].

Recent surge of studies on CDW and superconductivity in atomically thin TMDs [16–31] has opened a new route to probe their intricate interplay. 2*H*-TaS_2, with bulk CDW and superconducting transitions at 75 and 0.8 K, respectively, exhibits a peculiarly enhanced T_c up to 3 K as the thickness is reduced [25–27]. However, the origin of this unusual trend in T_c (reversed with respect to most layered superconductors) and whether TaS_2 preserves its CDW order in the monolayer limit remain debated. Resistivity measurements in exfoliated monolayers capped with boron nitride show the absence of CDW signature, and ascribe the rise of T_c to suppression of the CDW [26]. On the other hand, scanning tunneling measurements in samples epitaxially grown on graphene determine a 3×3 CDW superstructure [28,29], in line with the ordering vector $\mathbf{q}_{\mathrm{CDW}} = \frac{2}{3}\Gamma\mathrm{M}$ predicted for a freestanding monolayer from *ab initio* [30]. To date, it is still unclear if the intrinsic superconductivity of monolayer 1*H*-TaS_2 occurs in a coexisting CDW state. Also, TaS_2 in the monolayer limit has an enhanced in-plane upper critical field arising from Ising pairing dictated by antisymmetric spin-orbit coupling (SOC) [27,31], but how this SOC modulates its electron-phonon and superconducting properties is elusive. It is thus of great significance to clarify the essential roles of CDW and SOC in superconductivity and the associated enhancement mechanism inherent in Ta-based TMDs, compared to an interfacial mode coupling found in monolayer FeSe/$SrTiO_3$ [32]. In addition, examining the

*cslian@zzu.edu.cn

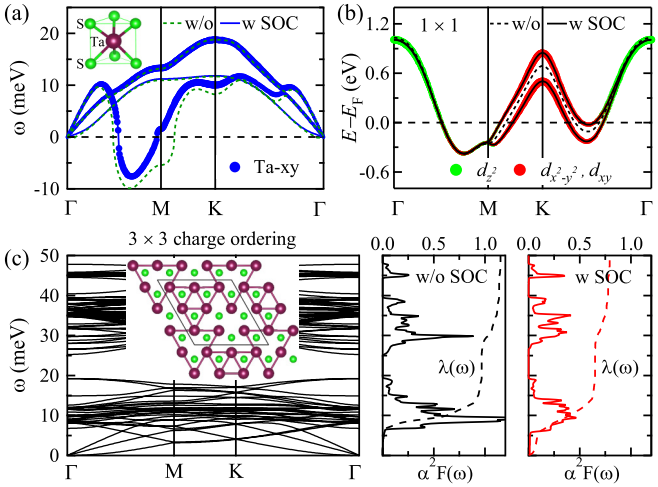

FIG. 1. (a) Acoustic phonon spectrum and (b) electronic band structure in the normal state of monolayer $1H$-TaS_2 with trigonal prismatic structure. (c) Phonon spectrum in the CDW state with its Eliashberg function $\alpha^2F(\omega)$ and integrated EPC $\lambda(\omega)$. Inset: Optimized 3×3 distorted structure.

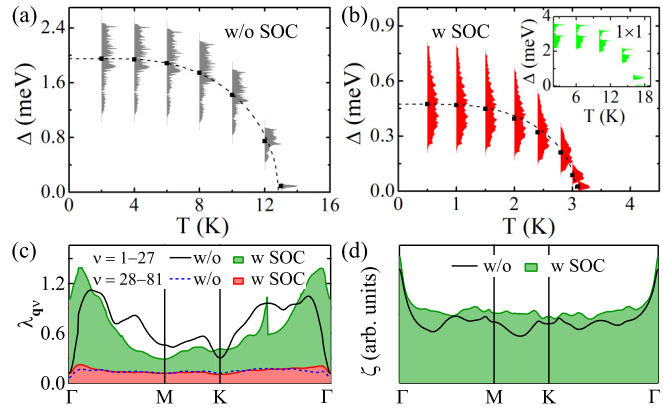

FIG. 2. [(a), (b)] Superconducting gap $\Delta_{\mathbf{k}}$ distribution versus temperature for monolayer TaS_2's CDW phase calculated without (a) and with SOC (b) using the anisotropic Migdal-Eliashberg theory. The black squares indicate the average value of the gaps and the dashed lines are fits obtained by solving numerically the BCS gap equation using the average Δ_0 and T_c from *ab initio* calculations. Inset in (b) shows the $\Delta_{\mathbf{k}}$ data for monolayer TaS_2's normal phase. (c) The mode-resolved EPC strength $\lambda_{\mathbf{q}\nu}$ and (d) the Fermi-surface nesting function ζ calculated without (black curves) and with SOC (shaded areas) for monolayer TaS_2's CDW phase.

effects of gate-introduced carrier doping on different quantum states in $1H$-TaS_2 will not only help understand their interactions but also provide a basis for controlling correlated orders in related two-dimensional devices.

In this Letter, we systematically investigate the superconductivity and its interplay with CDW order both in pristine and doped monolayer $1H$-TaS_2 using state-of-the-art *ab initio* calculations and the anisotropic Migdal-Eliashberg theory [33–37]. We verify a stable 3×3 CDW ground state for $1H$-TaS_2 by addressing anharmonic effects and unveil its distorted atomic structure. We show that SOC largely modifies the electron-phonon coupling (EPC) strength of this CDW phase, which is vital for reproducing the experimental superconducting T_c of monolayer TaS_2. The CDW is found to be weakened to 2×2 by electron doping, yielding increased EPC and T_c up to 11 K, while upon hole doping it remains robust coexisting with a still enhanced superconducting order. Combined with the concurrent evolution of CDW and superconductivity in the reduced dimensionality showing a cooperative behavior, our results demonstrate diversified mutual interactions between the two orders in ultrathin TaS_2 relying on specific control conditions.

The phonon spectrum and electronic band structure calculated for $1H$-TaS_2 monolayer in the normal state are shown in Figs. 1(a) and 1(b). The longitudinal acoustic (LA) phonon branch displays strongest instability at $\mathbf{q} = \frac{2}{3}\Gamma\mathrm{M}$ irrespective of the inclusion of SOC (inducing spin-split Ta d bands). This signifies a CDW order with 3×3 periodicity as commonly found in $2H$ group V TMDs [38–41], in accord with previous study adopting the harmonic approximation [30]. Anharmonic effects had been known to tend to suppress the CDW instability, especially for light disulfides like NbS_2 [42–44]. To check if charge ordering really exists, we calculate the anharmonic potential of the softest mode for the 3×3 supercell of monolayer TaS_2 and obtain an unsymmetric double-well potential that is deep enough to support a bound state in the deeper of the two wells (Fig. S1 in the Supplemental Material, SM [45]), in contrast to NbS_2 case where the ground-state wavefunction is centered in a very shallow symmetric double well [42]. Therefore, $1H$-TaS_2 has a robust CDW ground state at low temperature, consistent with recent measurements in monolayer samples prepared on graphene [28,29] or from thermal annealing of $1T$-TaS_2 surface [46].

Following the lowest-energy mode or through full optimization, we find the most stable CDW structure of $1H$-TaS_2 to be a 3×3 distorted phase displaying a continuous pattern of overlapping triangular six-atom Ta clusters centered on hollow sites [see inset of Fig. 1(c)]. Figure 1(c) shows the phonon spectrum of the CDW phase along with its Eliashberg function $\alpha^2F(\omega)$. The total EPC $\lambda = 2\int_0^\infty \alpha^2F(\omega)/\omega d\omega$, whose $\sim$80% is accounted for by the low-energy Ta modes below 20 meV, falls from 1.15 to 0.79 after including the SOC, implying a crucial role SOC plays in determining the superconductivity.

Figures 2(a) and 2(b) show the energy distribution of temperature-dependent superconducting gaps $\Delta_{\mathbf{k}}$ on the Fermi surface calculated for monolayer TaS_2's CDW phase without and with SOC using the Migdal-Eliashberg theory. In both cases an anisotropic single gap structure is formed. In the absence of SOC [Fig. 2(a)], the averaged superconducting gap is seen to vanish at a critical temperature $T_c = 13$ K, much higher than $3 - 3.4$ K reported in recent experiments [26,27]. However, once SOC is taken into account [Fig. 2(b)], accompanied by the decrease of total EPC [Fig. 1(c)], the resulting T_c is dramatically reduced to 3.1 K, very close to the experimental data, with an average gap of $\Delta_0 = 0.47$ meV in the zero-temperature limit. The detailed impact of SOC is clarified by analyzing the mode-resolved EPC strength $\lambda_{\mathbf{q}\nu}$ and the Fermi-surface nesting function ζ, which is proportional to $\lambda_{\mathbf{q}\nu}$ when adopting constant electron-phonon matrix elements

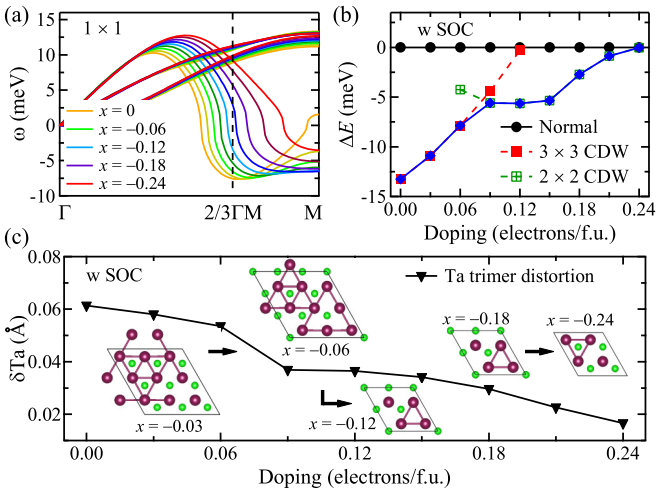

FIG. 3. (a) Evolution of acoustic phonons of monolayer $1H$-TaS_2 under electron doping (x in e/f.u.). (b) CDW formation energy ΔE (the 2×2 ΔE is scaled up to the 3×3 one) and (c) the Ta trimer distortion δTa toward a hollow site or a S atom of the CDW phase as a function of doping. Blue diamond lines in (b) represent the lowest-energy CDW structure at each doping level, as depicted in insets of (c) [49].

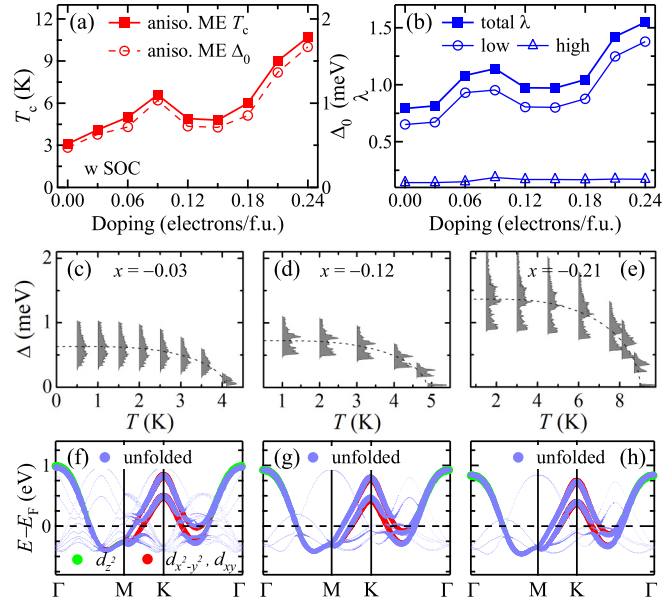

FIG. 4. [(a),(b)] Variation with electron doping of the T_c and Δ_0 derived from the anisotropic Migdal-Eliashberg theory (a) and the total λ (b) for monolayer TaS_2's CDW phase. [(c)−(e)] Superconducting gap $\Delta_{\mathbf{k}}$ distribution versus temperature of the CDW phase at $x = -0.03$, -0.12, and -0.21. [(f)−(h)] Unfolded band structure (blue dots) in the 1×1 Brillouin zone for the CDW phase at these three dopings, overlaid on the band structure of the corresponding undistorted phase.

$g^{\nu}_{\mathbf{q}}$. Upon the inclusion of SOC, $\lambda_{\mathbf{q}\nu}$ for the low-energy modes $\nu = 1 - 27$, folded from 1×1 phase's three acoustic modes, is reduced in most region of the Brillouin zone [Fig. 2(c)] [47], whereas that for the higher optical modes barely changes. Meanwhile, ζ slightly increases compared to the case without SOC [Fig. 2(d)]. These facts suggest it is those acoustic-like Ta-dominated phonon modes that are responsible for weakening the EPC strength via the SOC-induced suppression of their matrix elements. Similar modifications of λ and T_c are found in monolayer $NbSe_2$'s CDW phase (Table S1 and Fig. S2 in Supplemental Material [45]), demonstrating the general importance of SOC for correctly describing superconductivity in group V TMDs.

Prior work ascribed the enhanced T_c in $1H$-TaS_2 with respect to the bulk to the suppression of charge ordering in monolayer limit based only on CDW transport signal's disappearance [26]. Here, we find that for TaS_2's normal phase, which is stabilized under SOC with a large smearing of 0.03 Ry (compared to 0.01 Ry used in other cases), the superconducting T_c reaches 16.5 K [see inset of Fig. 2(b)], seriously deviating from the experiments. Thus, on top of SOC, consideration of the CDW order, which strongly interplays with superconductivity, is indispensable for reproducing $1H$-TaS_2's behavior. Notably, the $\Delta_{\mathbf{k}}$ distribution of its normal phase displays a two-gap structure as seen in NbS_2 and $NbSe_2$ [42,48] [inset of Fig. 2(b)], made of a large gap from in-plane $d_{x^2-y^2}$ and d_{xy} orbitals and a small one from out-of-plane d_{z^2} orbitals, while the single superconducting gap feature in TaS_2's CDW phase results from CDW-induced extensive energy gaps around K pockets where the Ta in-plane d states prevail, Fig. 1(b) (and Fig. S3 in Supplemental Material [45]).

Next we investigate the effects of charge doping on CDW and superconductivity in monolayer $1H$-TaS_2. With increasing electron doping [Fig. 3(a)], the wave vector of LA phonon branch's leading instability shifts from $\frac{2}{3}\Gamma$M to M, implying a transition of CDW order from 3×3 to 2×2. We determine the low-energy CDW structures at each doping level by performing full optimization of 3×3 or 2×2 superstructures with randomized distortions, and calculate their corresponding formation energy ΔE. As found in Figs. 3(b) and 3(c), at $x = -0.03$ and -0.06 e/f.u. doping levels the 3×3 CDW persists, while at $x = -0.09$ and higher levels the 2×2 CDW takes over as the ground state (Fig. S4 in Supplemental Material [45]). Overall, the energy gain $|\Delta E|$ due to the formation of CDW decreases with increasing doping, indicating a gradually weakened CDW. The suppression of charge ordering upon electron doping is reflected by both the decrease of Ta sublattice distortion [Fig. 3(c)] and the increase of Fermi-level density of states (DOS) N_F in the CDW state (Fig. S5 in Supplemental Material [45]).

Along with the weakening of competing CDW, we find the EPC strength and superconductivity in $1H$-TaS_2 to get significantly enhanced under electron doping. Figure 4(a) summarizes the variation of superconducting T_c and gap Δ_0 derived from the Migdal-Eliashberg theory with doping. Both T_c and Δ_0 show a doping dependence following the trend of total λ [Fig. 4(b)], with the former first peaking at $T_c = 6.6$ K for $x = -0.09$ and reaching the highest $T_c = 10.7$ K for $x = -0.24$, which exceeds $T_c \approx 9$ K achieved in pressurized $2H$-TaS_2 [10–12]. The dependence of λ is dictated by the contribution of low-energy phonon modes dominating the EPC in CDW state, which are directly affected by the Ta sublattice CDW distortion diminishing upon doping (see Figs. S5 and S6 in Supplemental Material [45]). In 3×3 CDW state, λ

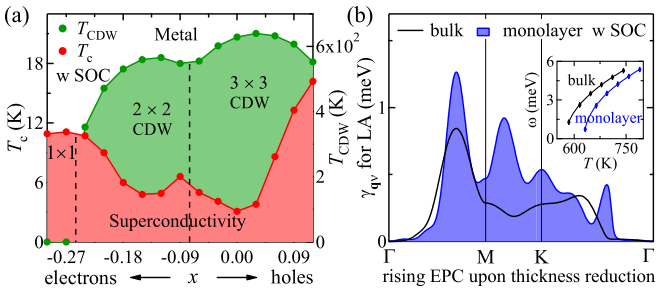

FIG. 5. (a) Doping-temperature phase diagram for monolayer $1H$-TaS_2. (b) Enhanced EPC ($\gamma_{\mathbf{q}\nu}$) of the soft LA branch from bulk to monolayer TaS_2, along with a rising T_{CDW} in the latter (inset) obtained via the mean-field fit of temperature-dependent soft-mode energies at $\mathbf{q} = \frac{2}{3}\Gamma M$.

increases with the applied doping as the E' mode softens. By contrast, λ in the subsequent 2×2 CDW state first decreases and then increases steadily; this dependence is closely related to the behaviors of N_F in the CDW state and its A_1'/E' modes, which exhibit almost opposite trends over the doping range for 2×2 CDW yielding their cooperative effect to λ.

Interestingly, with increasing electron doping, the superconducting gap of monolayer TaS_2's CDW phase exhibits a single-gap to two-gap transition. In comparison with the single anisotropic gap structure at $x = -0.03$ [Fig. 4(c)], an approximately double-peak feature emerges in the energy distribution of $\Delta_{\mathbf{k}}$ at $x = -0.12$ [Fig. 4(d)], and when doping is increased to $x = -0.21$, two distinct sets of superconducting gaps are identified, displaying a two-gap structure [Fig. 4(e)]. To better understand the doping-induced variation of the gap structure, we analyze the unfolded band structure of the CDW phase [50] shown in Figs. 4(f)–4(h): At $x = -0.03$, the K pockets are still highly affected by CDW distortion leading to strong Fermi-surface gapping of $d_{x^2-y^2}$ and d_{xy} states and a single-gap structure as in the pristine case; going from $x = -0.12$ to -0.21, those originally CDW-gapped in-plane d states gradually recover as the CDW is suppressed, which in turn contribute to forming a separated larger superconducting gap. Hence, besides tuning the λ and T_c, CDW-modulated electronic properties also determine the gap characteristic of doped superconducting TaS_2 systems.

To explore the interplay of CDW order with superconductivity in depth, we further evaluate the CDW transition temperature T_{CDW} under both electron and hole dopings by calculating the energy of $1H$-TaS_2's soft LA mode with Fermi-Dirac smearing (here the smearing value represents the electronic temperature). We obtain T_{CDW} by fitting the resulting soft-mode energy versus temperature data (Table S2 and Fig. S7 in Supplemental Material [45]) according to the mean-field formula [51,52]

$$\omega(T) = \omega_0(T/T_{CDW} - 1)^{\delta}. \quad (1)$$

Note that the T_{CDW} determined via Eq. (1) is useful to study the trends of CDW although it does overestimate measured transition temperatures [38]. Figure 5(a) summarizes the dependence of T_{CDW} and T_c in the doping-temperature phase diagram. Clearly, in electron doping case, T_{CDW} and T_c show an almost mirrored behavior until the CDW vanishes, in accord with the competitive interaction discussed earlier. Upon hole doping, however, T_{CDW} changes little below $x = 0.09$ while the T_c substantially increases to 13.3 K because of a particularly large N_F and total EPC ($\lambda = 1.72$) in the 3×3 CDW state. At $x = 0.15$ an intriguing 4×4 CDW emerges as the ground state, which remains robust against higher hole doping with a persisting superconducting order (see Figs. S8 and S9 in Supplemental Material [45]). These results suggest under different doping conditions the CDW could compete or nicely coexist with superconductivity, depending on the detailed CDW electronic structure, phonon modes and electron-phonon interaction. It is worth noting that in the strong-coupling limit ($\lambda \approx 2$) CDW and superconducting orders could be intertwined in a nonperturbative way [53], and the Migdal-Eliashberg theory may become invalid for evaluating T_c in highly doped systems. In fact, several methods have proven to significantly change the carrier density in CDW metals, such as gate-controlled Li ion intercalation [19] and ionic liquid gating [20]. We can conclude that the control of charge doping enables the manipulation of both CDW and superconducting states in monolayer $1H$-TaS_2. This flexibility is promising for application in controllable quantum devices based on the delicate interplay between the two correlated states as demonstrated here.

Finally, the origin of the T_c increase in the TaS_2 monolayer limit is suggested to be the enhancement of EPC due to cooperative interactions between CDW and superconductivity upon thickness reduction. This mechanism is more practical than previous proposals linked to a reduced Coulomb repulsion [25], weakening of CDW order [26], or opening of a second superconducting gap [54]), as it can be evidenced by our calculated monolayer $\lambda = 0.79$ being considerably larger than the bulk λ upper limit of 0.48 evaluated from the inverted McMillan equation [45,55]. Such an enhanced total EPC in CDW state correlates closely with a rising T_{CDW} from bulk to monolayer and an associated increase in the EPC of the soft LA branch in normal state, Fig. 5(b) (and Fig. S10 in Supplemental Material [45]). This phonon branch, which dictates the CDW, exhibits the largest electron-phonon matrix elements among all acoustic branches of the normal phase, and the evolution of its original EPC is expected to synchronously affect the EPC strength of the CDW phase contributed mainly by the low-energy CDW folded acoustic-like modes. Through this cooperativity, the CDW would readily boost superconductivity under reduced dimensionality [56]. We notice that given the varied sample conditions [25–29], besides the above cooperative scenario, whether other possibilities like substrate interfacial coupling are also at play for raising the T_c in monolayer limit remains open.

In conclusion, we have elucidated the intrinsic and doping-enhanced superconductivity in monolayer $1H$-TaS_2 within the *ab initio* anisotropic Migdal-Eliashberg theory. A persisting 3×3 CDW is confirmed in the monolayer, in which its experimentally observed T_c is successfully explained by addressing the marked weakening of electron-phonon interaction by SOC. This SOC-induced EPC renormalization is also significant in $1H$-$NbSe_2$, suggesting its universality in superconducting group V TMDs. It is found that, upon electron doping, superconductivity can largely be enhanced as CDW diminishes to 2×2, with an accompanying single-gap

to two-gap transition due to doping-induced suppression of the CDW gap. Strikingly, a low hole doping barely affects the coexisting CDW order but still yields substantially increased EPC and T_c. A probable cooperative behavior of CDW and superconductivity is also unveiled when thinning TaS_2 to monolayer limit. Our work highlights the complex interplay of the two collective orders in ultrathin $2H$-TaS_2, being competition, coexistence or cooperation depending on external stimuli or control, and offers key insights into the rich quantum phases of other CDW metals.

This work was supported by the National Natural Science Foundation of China (Grants No. 11904325, No. 11874079, and No. 51788104), the Ministry of Science and Technology of China (Grant No. 2016YFA0301001), and the National Supercomputing Center in Zhengzhou. C.H. and F.G. acknowledge support by the Austrian Science Fund (FWF) Project No. P 32144-N36 and the U.S. Department of Energy (DOE), Office of Science, Basic Energy Sciences (BES) under Award No. DE-SC0020129, respectively.

[1] J. A. Wilson, F. J. DiSalvo, and S. Mahajan, Adv. Phys. **50**, 1171 (2001).
[2] A. H. Castro Neto, Phys. Rev. Lett. **86**, 4382 (2001).
[3] J. Chang, E. Blackburn, A. T. Holmes, N. B. Christensen, J. Larsen, J. Mesot, R. Liang, D. A. Bonn, W. N. Hardy, A. Watenphul *et al.*, Nat. Phys. **8**, 871 (2012).
[4] E. H. da Silva Neto, P. Aynajian, A. Frano, R. Comin, E. Schierle, E. Weschke, A. Gyenis, J. Wen, J. Schneeloch, Z. Xu *et al.*, Science **343**, 393 (2014).
[5] B. Sipos, A. F. Kusmartseva, A. Akrap, H. Berger, L. Forró, and E. Tutiš, Nat. Mater. **7**, 960 (2008).
[6] R. Ang, Y. Tanaka, E. Ieki, K. Nakayama, T. Sato, L. J. Li, W. J. Lu, Y. P. Sun, and T. Takahashi, Phys. Rev. Lett. **109**, 176403 (2012).
[7] Y. Liu, R. Ang, W. J. Lu, W. H. Song, L. J. Li, and Y. P. Sun, Appl. Phys. Lett. **102**, 192602 (2013).
[8] K. E. Wagner, E. Morosan, Y. S. Hor, J. Tao, Y. Zhu, T. Sanders, T. M. McQueen, H. W. Zandbergen, A. J. Williams, D. V. West, and R. J. Cava, Phys. Rev. B **78**, 104520 (2008).
[9] L. Li, X. Deng, Z. Wang, Y. Liu, M. Abeykoon, E. Dooryhee, A. Tomic, Y. Huang, J. B. Warren, E. S. Bozin *et al.*, npj Quantum Mater. **2**, 11 (2017).
[10] D. C. Freitas, P. Rodière, M. R. Osorio, E. Navarro-Moratalla, N. M. Nemes, V. G. Tissen, L. Cario, E. Coronado, M. García-Hernández, S. Vieira, M. Núñez-Regueiro, and H. Suderow, Phys. Rev. B **93**, 184512 (2016).
[11] R. Grasset, Y. Gallais, A. Sacuto, M. Cazayous, Samuel Mañas-Valero, E. Coronado, and M.-A. Méasson, Phys. Rev. Lett. **122**, 127001 (2019).
[12] Y. Kvashnin, D. VanGennep, M. Mito, S. A. Medvedev, R. Thiyagarajan, O. Karis, A. N. Vasiliev, O. Eriksson, and M. Abdel-Hafiez, Phys. Rev. Lett. **125**, 186401 (2020).
[13] C.-W. Chen, J. Choe, and E. Morosan, Rep. Prog. Phys. **79**, 084505 (2016).
[14] M. Calandra and F. Mauri, Phys. Rev. Lett. **106**, 196406 (2011).
[15] H. Yang, S. W. Kim, M. Chhowalla, and Y. H. Lee, Nat. Phys. **13**, 931 (2017).
[16] M. M. Ugeda, A. J. Bradley, Y. Zhang, S. Onishi, Y. Chen, W. Ruan, C. Ojeda-Aristizabal, H. Ryu, M. T. Edmonds, H.-Z. Tsai *et al.*, Nat. Phys. **12**, 92 (2016).
[17] R. Bianco, L. Monacelli, M. Calandra, F. Mauri, and I. Errea, Phys. Rev. Lett. **125**, 106101 (2020).
[18] D. Lin, S. Li, J. Wen, H. Berger, L. Forró, H. Zhou, S. Jia, T. Taniguchi, K. Watanabe, X. Xi, and M. S. Bahramy, Nat. Commun. **11**, 2406 (2020).
[19] Y. Yu, F. Yang, X. F. Lu, Y. J. Yan, Y.-H. Cho, L. Ma, X. Niu, S. Kim, Y.-W. Son, D. Feng *et al.*, Nat. Nanotechnol. **10**, 270 (2015).
[20] X. Xi, H. Berger, L. Forró, J. Shan, and K. F. Mak, Phys. Rev. Lett. **117**, 106801 (2016).
[21] X. Xi, L. Zhao, Z. Wang, H. Berger, L. Forró, J. Shan, and K. F. Mak, Nat. Nanotechnol. **10**, 765 (2015).
[22] Y. Xing, K. Zhao, P. Shan, F. Zheng, Y. Zhang, H. Fu, Y. Liu, M. Tian, C. Xi, and H. Liu *et al.*, Nano Lett. **17**, 6802 (2017).
[23] H. Ryu, Y. Chen, H. Kim, H.-Z. Tsai, S. Tang, J. Jiang, F. Liou, S. Kahn, C. Jia, A. A. Omrani *et al.*, Nano Lett. **18**, 689 (2018).
[24] J. Bekaert, E. Khestanova, D. G. Hopkinson, J. Birkbeck, N. Clark, M. Zhu, D. A. Bandurin, R. Gorbachev, S. Fairclough, Y. Zou *et al.*, Nano Lett. **20**, 3808 (2020).
[25] E. Navarro-Moratalla, J. O. Island, S. Mañas-Valero, E. Pinilla-Cienfuegos, A. Castellanos-Gomez, J. Quereda, G. Rubio-Bollinger, L. Chirolli, J. A. Silva-Guillén, N. Agraït *et al.*, Nat. Commun. **7**, 11043 (2016).
[26] Y. Yang, S. Fang, V. Fatemi, J. Ruhman, E. Navarro-Moratalla, K. Watanabe, T. Taniguchi, E. Kaxiras, and P. Jarillo-Herrero, Phys. Rev. B **98**, 035203 (2018).
[27] S. C. de la Barrera, M. R. Sinko, D. P. Gopalan, N. Sivadas, K. L. Seyler, K. Watanabe, T. Taniguchi, A. W. Tsen, X. Xu, D. Xiao *et al.*, Nat. Commun. **9**, 1427 (2018).
[28] J. Hall, N. Ehlen, J. Berges, E. van Loon, C. van Efferen, C. Murray, Malte Rösner, J. Li, B. V. Senkovskiy, and M. Hell *et al.*, ACS Nano **13**, 10210 (2019).
[29] H. Lin, W. Huang, K. Zhao, C. Lian, W. Duan, X. Chen, and S.-H. Ji, Nano Res. **11**, 4722 (2018).
[30] O. R. Albertini, A. Y. Liu, and M. Calandra, Phys. Rev. B **95**, 235121 (2017).
[31] C. E. Sanders, M. Dendzik, A. S. Ngankeu, A. Eich, A. Bruix, M. Bianchi, J. A. Miwa, B. Hammer, A. A. Khajetoorians, and P. Hofmann, Phys. Rev. B **94**, 081404(R) (2016).
[32] J. J. Lee, F. T. Schmitt, R. G. Moore, S. Johnston, Y. T. Cui, W. Li, M. Yi, Z. K. Liu, M. Hashimoto, Y. Zhang *et al.*, Nature (London) **515**, 245 (2014).
[33] E. R. Margine and F. Giustino, Phys. Rev. B **87**, 024505 (2013).
[34] F. Giustino, M. L. Cohen, and S. G. Louie, Phys. Rev. B **76**, 165108 (2007).
[35] S. Poncé, E. R. Margine, C. Verdi, and F. Giustino, Comput. Phys. Commun. **209**, 116 (2016).

[36] C.-S. Lian, C. Si, and W. Duan, Phys. Rev. B **100**, 235420 (2019).

[37] All calculations were performed within the generalized gradient approximation [57] to density functional theory. We employed the QUANTUM ESPRESSO package [58,59] for electronic structure and lattice dynamics calculations, where the effect of SOC was included. We used relativistic norm-conserving pseudopotentials [60,61] with a plane-wave cutoff of 50 Ry. For the slab model of monolayer 1H-TaS_2, a 12-Å thick vacuum layer was introduced, and the optimized lattice constant in normal state is $a = 3.34$ Å. The electronic and vibrational Brillouin zones were sampled using 24×24 and 12×12, 10×10 and 5×5, and 6×6 and 3×3 points for its normal, 2×2 CDW, and 3×3 CDW phases, respectively. The EPW code [33–35] was employed to calculate the superconducting gap and critical temperature. Electron-phonon matrix elements were interpolated [34,62] onto 60×60 (100×100) **k**-point and 30×30 (50×50) **q**-point grids for the 3×3 (2×2) CDW phase. The screened Coulomb pseudopotential is $\mu^* = 0.15$. The Matsubara frequency cutoff was set to 0.4 eV and the Dirac deltas were replaced by Lorentzians with widths of 37.5 meV for electrons and 0.05 meV for phonons. For the study of charge doping effects, electrons were added to or removed from the system along with a compensating uniform charged background.

[38] F. Weber, S. Rosenkranz, J. P. Castellan, R. Osborn, R. Hott, R. Heid, K. P. Bohnen, T. Egami, A. H. Said, and D. Reznik, Phys. Rev. Lett. **107**, 107403 (2011).

[39] C.-S. Lian, C. Si, and W. Duan, Nano Lett. **18**, 2924 (2018).

[40] J. Dai, E. Calleja, J. Alldredge, X. Zhu, L. Li, W. Lu, Y. Sun, T. Wolf, H. Berger, and K. McElroy, Phys. Rev. B **89**, 165140 (2014).

[41] C.-S. Lian, C. Heil, X. Liu, C. Si, F. Giustino, and W. Duan, J. Phys. Chem. Lett. **10**, 4076 (2019).

[42] C. Heil, S. Poncé, H. Lambert, M. Schlipf, E. R. Margine, and F. Giustino, Phys. Rev. Lett. **119**, 087003 (2017).

[43] M. Leroux, M. Le Tacon, M. Calandra, L. Cario, M.-A. Méasson, P. Diener, E. Borrissenko, A. Bosak, and P. Rodière, Phys. Rev. B **86**, 155125 (2012).

[44] R. Bianco, I. Errea, L. Monacelli, M. Calandra, and F. Mauri, Nano Lett. **19**, 3098 (2019).

[45] See Supplemental Material at http://link.aps.org/supplemental/10.1103/PhysRevB.105.L180505 for Figs. S1 − S11 and Tables S1 and S2.

[46] Z. Wang, Y.-Y. Sun, I. Abdelwahab, L. Cao, W. Yu, H. Ju, J. Zhu, W. Fu, L. Chu, H. Xu, and K. P. Loh, ACS Nano **12**, 12619 (2018).

[47] The increase and then sudden drop of $\lambda_{\mathbf{q}\nu}$ are related to numerical difficulties arising for small $|\mathbf{q}|$.

[48] F. Zheng and J. Feng, Phys. Rev. B **99**, 161119(R) (2019).

[49] The CDW at $x = -0.03$ has similar hollow-centered six-atom Ta clusters as in the nondoping case, while at $x = -0.06$ it changes into a CDW with overlapping six-atom Ta clusters centered by S atoms; going from $x = -0.09$ to -0.21 the CDW has hollow-centered Ta trimer, while at $x = -0.24$ it changes again into a CDW with S atom-centered Ta trimer. The CDW eventually vanishes at doping above $x = -0.24$.

[50] W. Ku, T. Berlijn, and C.-C. Lee, Phys. Rev. Lett. **104**, 216401 (2010).

[51] G. Grüner, *Density Waves in Solids*, (Perseus, Cambridge, MA, 1994).

[52] M. J. Rice and S. Strässler, Solid State Commun. **13**, 1931 (1973).

[53] I. Esterlis, S. A. Kivelson, and D. J. Scalapino, Phys. Rev. B **99**, 174516 (2019).

[54] E. F. Talantsev, W. P. Crump, J. O. Island, Y. Xing, Y. Sun, J. Wang, and J. L. Tallon, 2D Mater. **4**, 025072 (2017).

[55] W. McMillan, Phys. Rev. **167**, 331 (1968).

[56] The exact bulk λ calls for additional theoretical studies.

[57] J. P. Perdew, K. Burke, and M. Ernzerhof, Phys. Rev. Lett. **77**, 3865 (1996).

[58] P. Giannozzi, S. Baroni, N. Bonini, M. Calandra, R. Car, C. Cavazzoni, D. Ceresoli, G. L. Chiarotti, M. Cococcioni, I. Dabo *et al.*, J. Phys.: Condens. Matter **21**, 395502 (2009).

[59] S. Baroni, S. de Gironcoli, A. D. Corso, and P. Giannozzi, Rev. Mod. Phys. **73**, 515 (2001).

[60] D. R. Hamann, Phys. Rev. B **88**, 085117 (2013).

[61] M. Schlipf and F. Gygi, Comput. Phys. Commun. **196**, 36 (2015).

[62] A. A. Mostofi, J. R. Yates, Y.-S. Lee, I. Souza, D. Vanderbilt, and N. Marzari, Comput. Phys. Commun. **178**, 685 (2008).